

Efficient Small Template Iris Recognition System Using Wavelet Transform

Mohammed A. M. Abdullah

*Computer Engineering Department,
University of Mosul,
Mosul, 41002, Iraq*

m.am_86@yahoo.com

F. H. A. Al-Dulaimi

*Computer Engineering Department,
University of Mosul,
Mosul, 41002, Iraq*

fhali310@yahoo.com

Waleed Al-Nuaimy

*Department of Electrical Engineering and Electronics,
University of Liverpool,
Liverpool, L69 3GJ, UK*

wax@liv.ac.uk

Ali Al-Aataby

*Department of Electrical Engineering and Electronics,
University of Liverpool,
Liverpool, L69 3GJ, UK*

ali.al-aataby@liv.ac.uk

Abstract

Iris recognition is known as an inherently reliable biometric technique for human identification. Feature extraction is a crucial step in iris recognition, and the trend nowadays is to reduce the size of the extracted features. Special efforts have been applied in order to obtain low templates size and fast verification algorithms. These efforts are intended to enable a human authentication in small embedded systems, such as an Integrated Circuit smart card. In this paper, an effective eyelids removing method, based on masking the iris, has been applied. Moreover, an efficient iris recognition encoding algorithm has been employed. Different combination of wavelet coefficients which quantized with multiple quantization levels are used and the best wavelet coefficients and quantization levels are determined. The system is based on an empirical analysis of CASIA iris database images. Experimental results show that this algorithm is efficient and gives promising results of False Accept Ratio (FAR) = 0% and False Reject Ratio (FRR) = 1% with a template size of only 364 bits.

Keywords: Biometrics, Iris Recognition, Wavelets Transform, Feature Extraction, Pattern Recognition.

1. INTRODUCTION

The term "Biometrics" refers to a science involving the statistical analysis of biological characteristics. This measurable characteristic, biometric, can be physical, such as eye, face, retina vessel, fingerprint, hand and voice or behavioral, like signature and typing rhythm. Biometrics, as a form of unique person identification, is one of the subjects of research that is growing rapidly [1].

The advantages of unique identification using biometric features are numerous, such as fraud prevention and secure access control. Biometrics systems offer great benefits with respect to other authentication techniques. In particular, they are often more user friendly and can guarantee the physical presence of the user [1].

Iris recognition is one of the most reliable biometric technologies in terms of identification and verification performance. The iris is the colored portion of the eye that surrounds the pupil as depicted in Figure 1. It controls light levels inside the eye similar to the aperture on a camera. The round opening in the center of the iris is called the pupil. The iris is embedded with tiny muscles that dilate and constrict the pupil size. It is full of richly textured patterns that offer numerous individual attributes which are distinct even between the identical twins and between the left and right eyes of a person. Compared with other biometric features such as face and fingerprints, iris patterns are highly stable with time and unique, as the probability for the existence of two irises that are same is estimated to be as low as, one in 10^{72} [1,2].

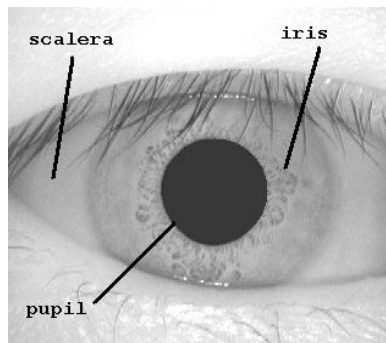


FIGURE 1: Image of the eye.

In this paper, the iris is efficiently normalized such that only useful data are encoded. Image enhancement techniques are applied. Moreover, the best combination of wavelet coefficients is found and used for successful identification and the best number of bits used for encoding the feature vector have been deduced while maintaining low template size.

The paper is organized as follows. Section 2 presents the main related works. Section 3 explains the typical stages of iris recognition and the proposed eyelid removing method. Section 4 presents the proposed feature extraction method. Experimental results are given in section 5, and Section 6 concludes this paper.

2. RELATED WORK

Iris identification using analysis of the iris texture has attracted a lot of attention and researchers have presented a variety of approaches in the literature.

Daughman [3] proposed the first successful implementation of an iris recognition system based on 2-D Gabor filter to extract texture phase structure information of the iris to generate a 2048 bits iris code. A group of researchers have used the 1-D wavelet transform as the core of the feature extraction module [4,5,6,7]. For instance, Boles and Boashash [4] extracted the features of the iris pattern by using the zero-crossings of 1-D wavelet transform of the concentric circles on the iris.

On the other hand, another group of researcher utilized 2-D wavelet transform to extract iris texture information [8,9,10,11,12,13,14]. For instance, Narote *et al* [11] proposed an algorithm for iris recognition based on dual tree complex wavelet transform and explored the speed and accuracy of the proposed algorithm. Hariprasath and Mohan [13] described iris recognition based on Gabor and Morlet wavelets such that the iris is encoded into a compact sequence of 2-D wavelet coefficient, which generate an iris code of 4096 bits. Kumar and Passi [14] presented a comparative study of the performance from the iris identification using different feature extraction methods with different templates size. Even though the previous systems have good recognition ratios, the template size remains rather large.

3. IRIS RECOGNITION SYSTEM

Generally, an iris recognition system is composed of many stages as shown in Figure 2. Firstly, an image of the person's eye is captured by the system and preprocessed. Secondly, the image is localized to determine the iris boundaries. Thirdly, the iris boundary coordinates are converted to the stretched polar coordinates to normalize the scale of the iris in the image. Fourthly, features representing the iris patterns are extracted based on texture analysis. Finally, the person is identified by comparing their features with an iris feature database.

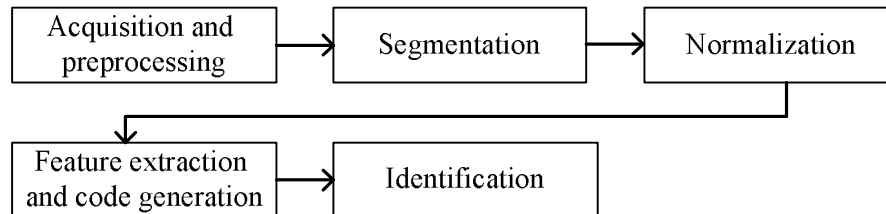


FIGURE 2: Block diagram of an iris recognition system.

3.1 Segmentation

For the purpose of identification, the part of the eye image carrying useful information is only the iris that lies between the sclera and the pupil [2]. Therefore, prior to performing iris matching, it is very important to localize the iris in the acquired image. The iris region, shown in Figure 3, is bounded by two circles, one for the boundary with the sclera and the other, interior to the first, with the pupil.

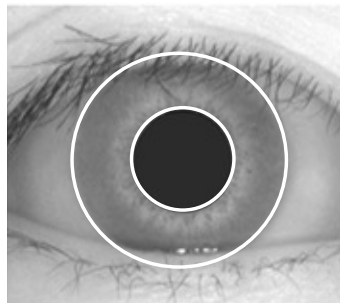


FIGURE 3: Segmented eye image.

To detect these two circles the Circular Hough transform (CHT) has been used. The Hough transform is a standard computer vision algorithm that can be used to determine the geometrical parameters for a simple shape, present in an image, and this has been adopted here for circle detection [15]. The main advantage of the Hough transform technique is its tolerance for gaps in feature boundary descriptions and its robustness to noise [16].

Basically, the first derivatives of intensity values in an eye image are calculated and the result is used to generate an edge map. From the edge map, votes are cast in Hough space for the parameters of circles passing through each edge point. These parameters are the center coordinates x_c and y_c , and the radius r , which are able to define any circle according to the following equation:

$$x_c^2 + y_c^2 - r^2 = 0 \quad \dots (1)$$

A maximum point in the Hough space will correspond to the radius and center coordinates of the best circle defined by the edge points [15].

3.2 Normalization

The size of the iris varies from person to person, and even for the same person, due to variation in illumination, pupil size and distance of the eye from the camera. These factors can severely affect iris matching results. In order to get accurate results, it is necessary to eliminate these factors. To achieve this, the localized iris is transformed into polar coordinates by remapping each point within the iris region to a pair of polar coordinates (r, θ) where r is in the interval $[0, 1]$ with 1 corresponding to the outermost boundary and θ is the angle in the interval $[0, 2\pi]$ as shown in Figure 4 [17,18].

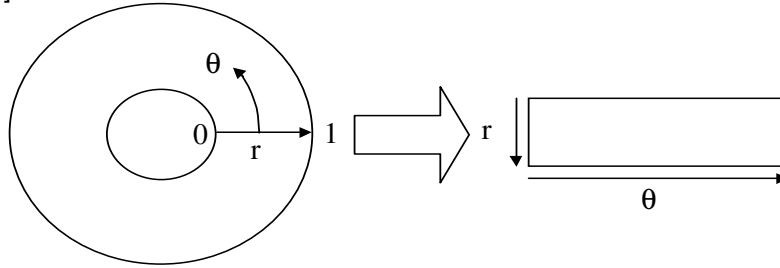


FIGURE 4: Rubber sheet model [17].

With reference to Figure 5, the remapping of the iris region from (x,y) Cartesian coordinates to the normalized non-concentric polar representation is modeled by the following equations:

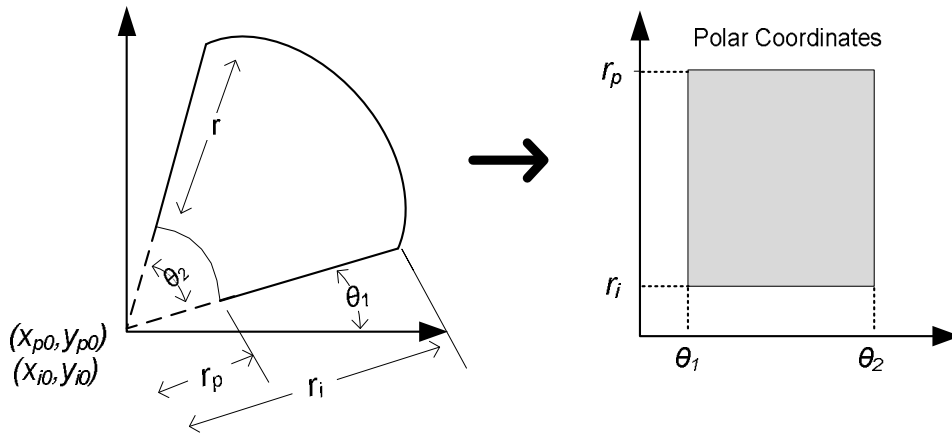


FIGURE 5: Image mapping from Cartesian coordinates to dimensionless polar coordinates.

$$I(x(r, \theta), y(r, \theta)) \rightarrow I(r, \theta) \quad \dots (2)$$

$$x(r, \theta) = (1 - r)x_p(\theta) + rx_i(\theta) \quad \dots (3)$$

$$y(r, \theta) = (1 - r)y_p(\theta) + ry_i(\theta) \quad \dots (4)$$

with

$$x_p(r, \theta) = x_{p0}(\theta) + r_p \cos \theta \quad \dots (5)$$

$$y_p(r, \theta) = y_{p0}(\theta) + r_p \sin \theta \quad \dots (6)$$

$$x_i(r, \theta) = x_{i0}(\theta) + r_i \cos \theta \quad \dots (7)$$

$$y_i(r, \theta) = y_{i0}(\theta) + r_i \sin \theta \quad \dots (8)$$

Where I is the iris picture, r_p and r_i are respectively the radius of pupil and the iris, while $x_p(\theta), y_p(\theta)$ and $x_i(\theta), y_i(\theta)$ are the coordinates of the papillary and iris boundaries in the direction θ . (x_{p0}, y_{p0}) and (x_{i0}, y_{i0}) are the centers of pupil and iris respectively.

For a typical eye image of dimension 320×280 pixel, the previous normalization method is performed to produce 50 pixels along r and 600 pixels along θ which result in 600×50 unwrapped strip.

On account of asymmetry of pupil (*not being a circle perfectly*) and probability of overlapping outer boundaries with sclera, we select 45 pixels from 50 pixels along r in the unwrapped iris. Therefore, the unwrapped iris becomes of dimensions 600×45 . The normalized iris image is shown in Figure 6.

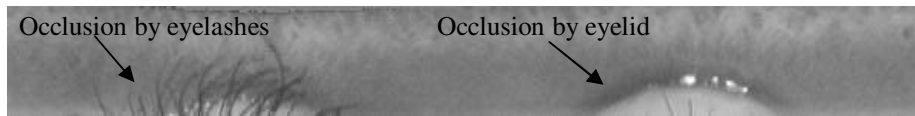


FIGURE 6: Normalized iris image.

3.3 Proposed Eyelash and Eyelid Removing Method

Since in most cases the upper and lower parts of the iris area are occluded by eyelids, it was decided to use only the left and right parts of the iris with a partial area of the upper and lower region for the iris recognition. Therefore, the whole iris $[0, 360^\circ]$ is not transformed in the proposed system. Experiments were conducted by masking the iris from $[148, 212^\circ]$ and $[328, 32^\circ]$ for the right and left parts while for the upper and lower parts, a semi circle with a radius equals to the half of the iris radius is used to mask the iris as depicted in Figure 7. Hence, the regions that contain the eyelids and eyelashes have been omitted while the remaining eyelashes are treated by thresholding, since analysis reveals that eyelashes are quite dark when compared with the rest of the eye image [15]. The corresponding rectangular block is show in Figure 8. Afterward, the block is concatenated together as shown in Figure 9.

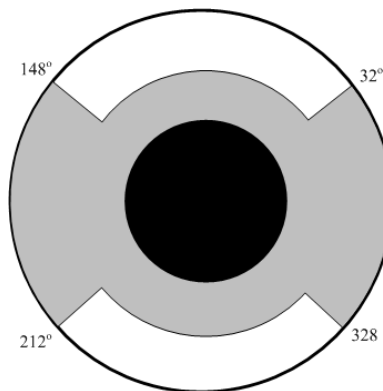


FIGURE 7: Masking the iris.



FIGURE 8: The normalized masked iris image.

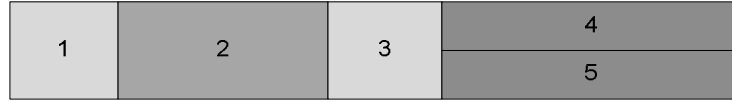


FIGURE 9: The concatenated block after removing the ignored parts.

The size of the rectangular block is reduced accordingly. By applying this approach, detection time of upper and lower eyelids and some cost of the polar transformation are saved. Saving ratio can be calculated from this equation:

$$\text{Saving ratio} = (\text{ignored parts of the iris} / \text{whole iris region}) * 100\% \quad \dots (9)$$

where

$$\begin{aligned} \text{ignored parts} &= ((148-32) + (328-212))/2 = 116 \\ \text{Saving rati}on &= 116/360 * 100\% = 32.22\% \end{aligned}$$

Figure 10 illustrates applying the proposed masking method on a normalized iris.

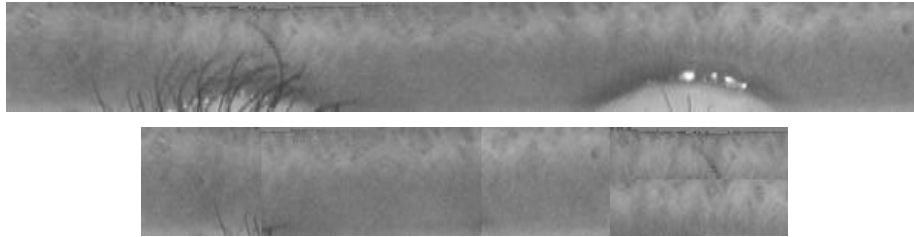


FIGURE 10: Applying the proposed masking method on a normalized iris.

Although the homogenous rubber sheet model accounts for pupil dilation and imaging distance it does not compensate for rotational inconsistencies. Rotational inconsistencies are treated in the matching stage (section 3.6).

3.4 Image Enhancement

Due to the effect of imaging conditions and situations of light sources, the normalized iris image does not have an appropriate quality. These disturbances may affect the performance of feature extraction and matching processes [12].

Hence for getting a uniform distributed illumination and better contrast in iris image, the polar transformed image is enhanced through adjusting image intensity values by mapping the intensity values in the input grayscale image to new values such that 1% of the pixel data is saturated at low and high intensities of the original image. This increases the contrast in a low-contrast grayscale image by remapping the data values to fill the entire intensity range [0, 255]. Then, histogram equalization has been used. Results of images before and after enhancement are shown in Figure 11.

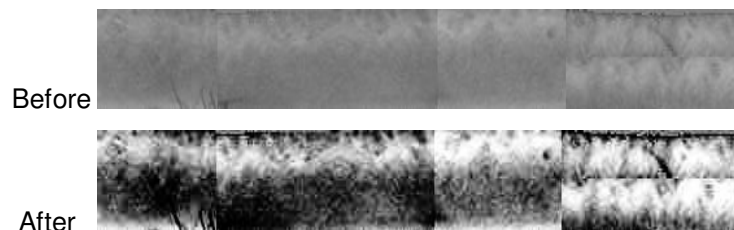


FIGURE 11: Image enhancement of the normalized iris.

3.5 Proposed Feature Extraction Method

In order to provide accurate recognition of individuals, the most discriminating information present in an iris pattern must be extracted. Only the significant features of the iris must be encoded so that comparisons between templates can be made. Most iris recognition systems make use of a band pass decomposition of the iris image to create a biometric template. For the encoding process the outputs of any used filter should be independent, so that there are no correlations in the encoded template, otherwise the filters would be redundant [19].

The Wavelet transform is used to extract features from the enhanced iris images. Haar wavelet is used as the mother wavelet. The Wavelet transform breaks an image down into four sub-sampled images. The results consist of one image that has been high-pass filtered in the horizontal and vertical directions (*HH* or Diagonal coefficients), one that has been low-pass filtered in the vertical and high-pass filtered in the horizontal (*LH* or Horizontal coefficients), one that has been low-pass filtered in the horizontal and high-pass filtered in the vertical (*HL* or Vertical coefficients), and one that has been low-pass filtered in both directions (*LL* or details coefficient) [8].

In Figure 12, a conceptual figure of basic decomposition steps for images is depicted. The approximation coefficients matrix *cA* and details coefficients matrices *cH*, *cV*, and *cD* (horizontal, vertical, and diagonal, respectively) obtained by wavelet decomposition of the input iris image. The definitions used in the chart are as follows [12].

- a. $C \downarrow$ denote downsample columns.
- b. $D \downarrow$ denote downsample rows.
- c. Lowpass_D denotes the decomposition low pass filter.
- d. Highpass_D denotes the decomposition high pass filter.
- e. *I_i* denotes the input image.

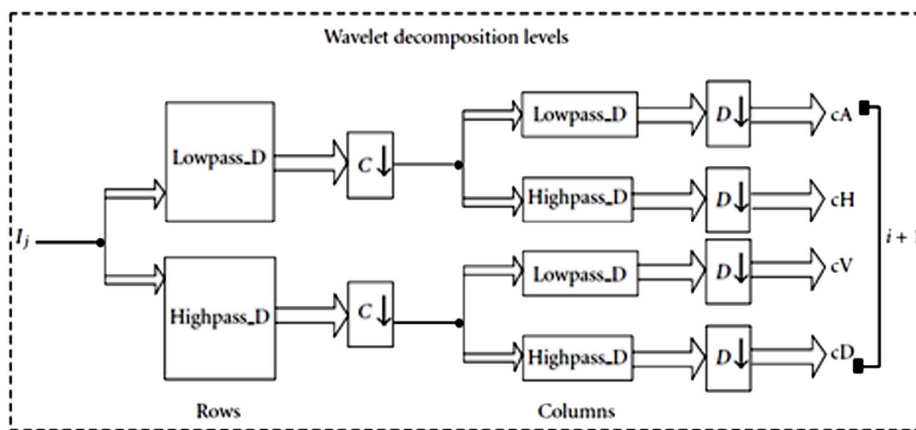


FIGURE 12: Wavelet decomposition steps diagram.

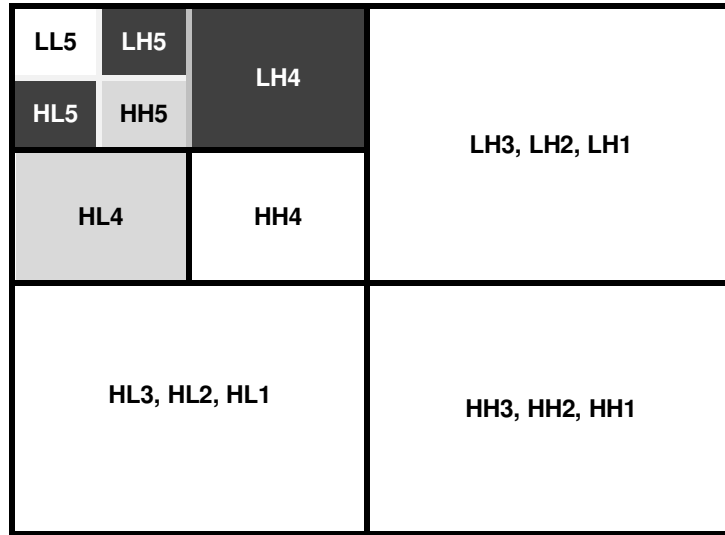


FIGURE 13: Five-level decomposition process with Haar wavelet. (Black indicates 4 levels quantization, Grey indicates two levels quantization).

Experiments were performed using different combinations of Haar wavelet coefficients and the results obtained from different combinations were compared to find the best. Since unwrapped image after masking has a dimension of 407×45 pixels, after 5 times decompositions, the size of the 5th level decomposition is 2×13 while for the 4th level is 3×26. Based on empirical experiments, the feature vector is arranged by combining features from *HL* and *LH* of level-4 (vertical and horizontal coefficients [*HL4 LH4*]) with *HL*, *LH* and *HH* of level-5 (vertical, horizontal and diagonal coefficients [*HL5 LH5 HH5*]). Figure 13 shows a five level decomposition with Haar wavelet.

In order to generate the binary data, features of *HL4* and *HH5* are encoded using two-level quantization while features of *LH4*, *HL5* and *LH5* are encoded using four-level quantization. After that these features are concatenated together as shown in Figure 14 which illustrates the process used for obtaining the final feature vector.

| | | | | |
|------------------------------------|---------------------------------|-----------------------------------|-----------------------------------|---------------------------------|
| LH4 156 bits 2×[3×26] | HL4 78 bits [3×26] | LH5 52 bits 2×[2×13] | HL5 52 bits 2×[2×13] | HH5 26 bits [2×13] |
|------------------------------------|---------------------------------|-----------------------------------|-----------------------------------|---------------------------------|

FIGURE 14: Organization of the feature vector which consists of 364 bits.

3.6 Matching

The last module of an iris recognition system is used for matching two iris templates. Its purpose is to measure how similar or different templates are and to decide whether or not they belong to the same individual or not. An appropriate match metric can be based on direct point-wise comparisons between the phase codes [18]. The test of matching is implemented by the Boolean XOR operator applied to the encode feature vector of any two iris patterns, as it detects disagreement between any corresponding pair of bits. This system quantifies this matter by computing the percentage of mismatched bits between a pair of iris representations, *i.e.*, the normalized Hamming distance.

Let *X* and *Y* be two iris representations to be compared and *N* be the total number

$$HD = \frac{1}{N} \sum_{j=1}^N X_j \oplus Y_j \quad \dots (10)$$

In order to avoid rotation inconsistencies which occur due to head tilts, the iris template is shifted right and left by 6 bits. It may be easily shown that scrolling the template in Cartesian coordinates is equivalent to an iris rotation in polar coordinates. This algorithm performs matching of two templates several times while shifting one of them to different locations. The smallest *HD* value amongst all these values is selected, which gives the matching decision [18, 19].

4. EXPERIMENTAL RESULTS AND COMPARISON

The images are obtained from the Chinese Academy of Sciences Institute of Automation (CASIA) [20] which is available in public domain. The database consists of 756 iris images from 108 classes. Images from each class are taken from two sessions with one month interval between the sessions. For each iris class, we choose three samples taken at the first session for training and all samples captured at the second session serve as test samples. This is also consistent with the widely accepted standard for biometrics algorithm testing [21, 22].

Experiments were performed using different combinations of wavelet coefficients and the results obtained from different combinations are compared to find the best as shown in Table 1. The selected combination gives the best Correct Recognition Rate (CRR) for a minimum feature vector length of 364 bits only.

| Combinations | Quantization | CRR | Vector Size |
|---|-------------------|-------|-------------|
| CH4 (D&V) | 2 bits | 69% | 156 bits |
| CH4 (V&H) | 2 bits | 73% | 156 bits |
| CH4 (D&H) | 2 bits | 70% | 156 bits |
| CH4 (D&V) + CH5 (V) | 2 bits | 76% | 182 bits |
| CH4 (D&V) + CH5 (H) | 2 bits | 82% | 182 bits |
| CH4 (D&V) + CH5 (D) | 2 bits | 77.8% | 182 bits |
| CH4 (D&V) + CH5 (D&V) | 2 bits | 83% | 208 bits |
| CH4 (D&V&H) | 2 bits | 85% | 162 bits |
| CH4 (H) + CH5 (H) | 4 bits | 92% | 208 bits |
| CH4 (H) + CH5 (V) | 4 bits | 89% | 208 bits |
| CH4 (H) + CH5 (V&H) | 4 bits | 95% | 260 bits |
| CH4 (D) + CH5 (V&H) | 4 bits | 72% | 260 bits |
| CH4 (V) + CH5 (V&H) | 4 bits | 68.5% | 260 bits |
| CH4 (D&H) | 4 bits | 92% | 312 bits |
| CH4 (D&V) | 4 bits | 62% | 312 bits |
| CH4 (V&H) | 4 bits | 88% | 312 bits |
| CH5 (V&H) | 4 bits | 54% | 312 bits |
| CH5 (V&D) | 4 bits | 49% | 312 bits |
| CH4 (V&H) + CH5 (V) | 4 bits | 90% | 368 bits |
| CH4 (V&H) + CH5 (H) | 4 bits | 93% | 368 bits |
| CH4 (D&V) + CH5 (D&V) | 4 bits | 71% | 416 bits |
| CH4 (V&H) + CH5 (V&D) | 4 bits | 90.5% | 416 bits |
| CH4 (V&H) + CH5 (V&H) | 4 bits | 96% | 416 bits |
| CH4 (V&D&H) | 4 bits | 91% | 468 bits |
| CH4 (H) ₄ + CH4 (V) ₂ CH5 (V) ₄ + CH5 (H) ₄ + CH5 (D) ₂ | 2 bits and 4 bits | 99% | 364 bit |

TABLE 1: Comparison among multiple wavelet coefficients
(D: Diagonal coefficients, H: Horizontal coefficients, and V: Vertical coefficients).

With a pre-determined separation Hamming distance, a decision can be made as to whether two templates were created from the same iris (*a match*), or whether they were created from different irises. However, the intra-class and inter-class distributions may have some overlap, which would result in a number of incorrect matches or false accepts, and a number of mismatches or false rejects. Table 2 shows the FAR and FRR associated with different separation points.

| Threshold | FAR (%) | FRR (%) |
|-----------|---------|---------|
| 0.20 | 0.00 | 59.34 |
| 0.24 | 0.00 | 28.80 |
| 0.26 | 0.00 | 10.30 |
| 0.28 | 0.00 | 3.87 |
| 0.29 | 0 | 1.00 |
| 0.30 | 1.51 | 0.86 |
| 0.32 | 5.43 | 0.00 |
| 0.36 | 26.47 | 0.00 |
| 0.38 | 48.68 | 0.00 |

TABLE 2: False accept and false reject rates for CASIA database with different separation points.

Figure 15 shows the distribution of inter-class and intra-class distribution of the system with a Hamming distance separation point of 0.29. With this separation point, false accept rate and false reject rate of 0% and 1% respectively are achieved. Such FRR are appeared, due to the overlap between the classes but it still allows for accurate recognition.

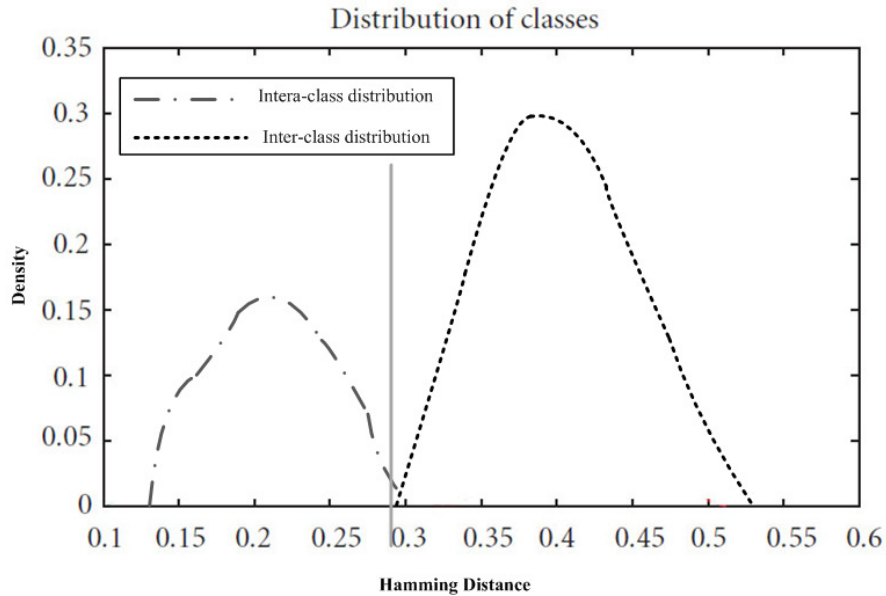


FIGURE 15: The distribution of intra-class and inter-class distances with a separation point of 0.29.

This system scored a perfect 0% FAR and 1% FRR. Table 3 shows the classification rate compared with a well known methods.

| Method | Feature Lengths (bits) | CRR (%) | Used Database |
|--------------------------|------------------------|---------|---------------|
| Narote <i>et al</i> [11] | 1088 | 99.2 | CASIA [20] |
| Poursaberi [12] | 544 | 97.22 | CASIA [20] |
| Hariprasath [13] | 4096 | 99.0 | UBIRIS [24] |
| Xiaofu [23] | 1536 | 98.15 | CASIA [20] |
| Proposed | 364 | 99.0 | CASIA [20] |

TABLE 3: Comparison of feature vector length and the Correct Recognition rate (CRR).

In the two methods; [11] and [13], the CRR is equal or a little bit better than ours. In fact, the dimensionality of the feature vector in both methods is much higher than ours. The feature vector consists of 1088 bits in [11] and of 4096 in [13], while it consists only of 364 bits in the proposed method. In addition, neither [11] nor [12] have suggested a method for removing eyelids or eyelashes.

Furthermore, [12] proposed a method to produce 544 bits of feature vector by applying four-level wavelet transform on the lower part of the iris assuming that only the upper part is occluded by the eyelashes and eyelids while the lower part is not. On the other hand, [23] employed two dimensional complex wavelet transform to produce 1536 bits of feature vector, however no method for noise removing has been applied also.

5. CONCLUSION

In this paper, we proposed an iris recognition algorithm using wavelet texture features based on a novel masking approach for eyelid removing. A masked area around the iris is used in the iris detection method. This area contains a complex and abundant texture information which are useful for feature extraction. The feature vector is quantized to a binary one, reducing the processing time and space, while maintaining the recognition rate.

Experimental results using CASIA database illustrate that relying on a smaller but more reliable region of the iris, although reduced the net amount of information, improve the recognition performance.

The experimental results clearly demonstrate that the feature vector consisting of concatenating *LH4*, *HL4*, *LH5*, *HL5*, and *HH5* gives the best results. On the other hand, Haar wavelet is particularly suitable for implementing high-accuracy iris verification/identification systems, as feature vector is at the least with respect to other wavelets. In identification mode, the CRR of the proposed algorithm was 99% with template size of 364 bits. Such vector size can be easily stored on smart cards and participate to reduce the matching and encoding time tremendously.

The proposed algorithm is characterized by having less computational complexity compared to other methods. Based on the comparison results shown in Table 3, it can be concluded that the proposed method is promising in terms of execution time and performance of the subsequent operations due to template size reduction.

6. REFERENCES

- [1] D. Woodward, M. Orlans and T. Higgins. *"Biometrics"*. McGraw-Hill, Berkeley, California, pp. 15-21 (2002)
- [2] H. Proença, A. Alexandre. *"Towards noncooperative iris recognition: A classification approach using multiple signatures"*. IEEE Transaction on Pattern Analysis, 29(4): 607-612, 2007
- [3] J. Daugman, *"High confidence visual recognition of persons by a test of statistical independence"*. IEEE Transaction on Pattern Analysis, 15(11): 1148-1161, 1993
- [4] W. Boles, B. Boashash. *"A Human Identification Technique Using Images of the Iris and Wavelet Transform"*. IEEE Transactions on Signal Processing, 46(4): 1085–1088, 1998
- [5] C. Chena, C. Chub. *"High Performance Iris Recognition based on 1-D Circular Feature Extraction and PSO–PNN Classifier"*. Expert Systems with Applications journal, 36(7): 10351-10356, 2009
- [6] H. Huang, G. Hu. *"Iris Recognition Based on Adjustable Scale Wavelet Transform"*. 27th Annual International Conference of the Engineering in Medicine and Biology Society, Shanghai, 2005
- [7] H. Huang, P.S. Chiang, J. Liang. *"Iris Recognition Using Fourier-Wavelet Features"*. 5th International Conference Audio- and Video-Based Biometric Person Authentication, Hilton Rye Town, New York, 2005
- [8] J. Kim, S. Cho, R. J. Marks. *"Iris Recognition Using Wavelet Features"*. The Journal of VLSI Signal Processing, 38(2): 147-156, 2004
- [9] S. Cho, J. Kim. *"Iris Recognition Using LVQ Neural Network"*. International conference on signals and electronic systems, Porzan, 2005

- [10] O. A. Alim, M. Sharkas. *"Iris Recognition Using Discrete Wavelet Transform and Artificial Neural Networks"*. IEEE International Symposium on Micro-Nano Mechatronics and Human Science, Alexandria, 2005
- [11] S.P. Narote, A.S. Narote, L.M. Waghmare, M.B. Kokare, A.N. Gaikwad. *"An Iris Recognition Based on Dual Tree Complex Wavelet Transform"*. TENCN IEEE 10th conference, Pune, India, 2007
- [12] A. Poursaberi, B.N. Araabi. *"Iris Recognition for Partially Occluded Images: Methodology and Sensitivity Analysis"*. EURASIP Journal on Advances in Signal Processing, 2007(1): 12-14, 2007
- [13] S. Hariprasath, V. Mohan. *"Biometric Personal Identification Based On Iris Recognition Using Complex Wavelet Transforms"*. Proceedings of the 2008 International Conference on Computing, Communication and Networking (ICCCN) IEEE, 2008
- [14] A. Kumar, A. Passi. *"Comparison and Combination of Iris Matchers for Reliable Personal Identification"*. Computer Vision and Pattern Recognition Workshops, IEEE, 2008
- [15] R. Wildes, J. Asmuth, G. Green, S. Hsu, and S. McBride. *"A System for Automated Iris Recognition"*, Proceedings IEEE Workshop on Applications of Computer Vision, Sarasota, FL, USA, 1994
- [16] T. Moravčík. *"An Approach to Iris and Pupil Detection in Eye Image"*. XII International PhD Workshop OWD, University of Žilina, Slovakia, 2010
- [17] K. Dmitry *"Iris Recognition: Unwrapping the Iris"*. The Connexions Project and Licensed Under the Creative Commons Attribution License, Version 1.3. (2004)
- [18] R. Schalkoff. *"Pattern Recognition: Statistical, Structural and Neural Approaches"*. John Wiley and Sons Inc., pp. 55-63 (2003)
- [19] J. Daugman. *"Statistical Richness of Visual Phase Information: Update on Recognizing Persons by Iris Patterns"*. International Journal of Computer Vision, 45(1): 25-38, 2001
- [20] Chinese Academy of Sciences, Center of Biometrics and Security Research. Database of 756 Grayscale Eye Images. <http://www.cbsr.ia.ac.cn/IrisDatabase.htm>
- [21] A. Mansfield and J. Wayman, *"Best practice standards for testing and reporting on biometric device performance"*. National Physical Laboratory of UK, 2002
- [22] L. Ma. *"Personal identification based on iris recognition"*. Ph.D. dissertation, Institute of Automation, Chinese Academy of Sciences, Beijing, China, 2003
- [23] H. Xiaofu, S. Pengfei. *"Extraction of Complex Wavelet Features for Iris Recognition"*. Pattern Recognition, 19th International Conference on Digital Object Identifier, Shanghai, 2008
- [24] Department of Computer Science, University of Beira Interior, Database of eye images. Version 1.0, 2004. <http://iris.di.ubi.pt/>